Journal of Constructional Steel Research 221 (2024) 108902

Contents lists available at ScienceDirect

Journal of Constructional Steel Research

journal homepage: www.elsevier.com/locate/jcsr

Seismic resilience comparison of CFST frame and HSS frame structures: An assessment based on economic and carbon emission indicators

Jiajun Du [a,b], Wei Wang [a,b,*], Shiye Wang [a,b]

[a] State Key Laboratory of Disaster Reduction in Civil Engineering & Department of Structural Engineering, Tongji University, Shanghai 200092, China
[b] Shanghai Engineering Research Center for Resilient Cities and Intelligent Disaster Mitigation, Tongji University, Shanghai 200092, China

ARTICLE INFO

Keywords:
Seismic resilience assessment
Carbon emission calculation
Concrete-filled steel tubular
Composite frame
Steel frame

ABSTRACT

This study presents a comparative seismic resilience assessment of concrete-filled steel tubular (CFST) frame structures and hollow structural steel (HSS) frame structures, focusing on economic and environmental aspects. Two comparable 9-story frame structures are designed: one with CFST columns and H-beams, the other with HSS columns and H-beams. The seismic resilience assessment is performed, incorporating hazard, structural, damage, and consequence analyses. In the structural analysis, the seismic performance of different structural systems is evaluated by employing the state-of-the-art numerical models. In consequence analysis, in addition to considering economic indicator, carbon emissions are also estimated using repair cost ratios and localized carbon emission factors in China. The findings reveal that under frequent and basis ground motions, CFST and HSS frames exhibit similar structural response, while CFST frames demonstrate lower collapse probabilities in rare and vary rare earthquake scenarios due to the concrete-filled tubes' ability to suppress buckling. Despite this, CFST columns may have less ductility than HSS columns, potentially leading to greater post-earthquake consequences. The life cycle seismic consequences evaluations indicate that CFST frame has less economic loss but higher carbon emissions. Overall, the CFST frame presents advantages in both economic and environmental aspects when initial costs and life cycle seismic consequences are combined. This study offers insights into the benefits and limitations of both the CFST column and HSS column in frame structures from the economic and environmental perspectives, offering a basis for sustainable and resilient structural design.

1. Introduction

According to the latest report by the United Nations Intergovernmental Panel on Climate Change (IPCC) [1], the anthropogenic emissions of greenhouse gases (GHG) continue to drive global warming, presenting an unprecedentedly severe challenge to human communities both in the present and for the future. The construction industry, as a major contributor to GHG emissions, has accordingly received significant attention. In 2020, the total carbon emissions from the entire construction process in China reached 5.08 billion tons of carbon emissions, accounting for 50.9% of the national carbon emissions [2]. Generally, carbon emissions from the construction industry can be typically categorized into direct, indirect, and embodied carbon emissions. The first two comprise the building's operational carbon emissions, while the latter includes emissions from construction activities (including the construction phase, maintenance during the use phase, and demolition at the end of a building's life) as well as emissions from the production of building materials. In China, embodied carbon emissions accounted for 57.4% of the construction industry's total carbon emissions in 2020, with 96.6% of these embodied emissions originating from the production of building materials [2]. Among all building materials, steel production contributed 1.47 billion tons of carbon emissions, constituting 52% of the total, while cement production accounted for 1.23 billion tons, making up 44% [2].

To alleviate the environmental footprint of steel and cement production, industries are actively promoting the development of these materials towards higher performance [3] (e.g., ultra-high-performance concrete [4] and high-strength steel [5,6]), recyclability (e.g., recycled concrete [7]), carbon sequestration (e.g., engineered wood [8]), and environmental durability (e.g., stainless steel [9]). However, compared to traditional materials, these alternatives currently come at a relatively higher cost and are still in the early stages of application [10]. In addition to enhancing the performance of individual materials, engineers also strive to create structural members with superior performance

* Corresponding author at: State Key Laboratory of Disaster Reduction in Civil Engineering, Tongji University, Shanghai 200092, China.
E-mail address: weiwang@tongji.edu.cn (W. Wang).

https://doi.org/10.1016/j.jcsr.2024.108902
Received 30 April 2024; Received in revised form 23 June 2024; Accepted 12 July 2024
Available online 27 July 2024

by integrating different materials rationally, such as concrete-filled steel tubular (CFST). The CFST is a composite member filled with concrete in steel tubes, which fully utilizes the advantages of both steel and concrete. The supporting effect of the internal concrete on the external tube can effectively improve the components' stability, bearing capacity, and fire resistance, while the confining effect of the external steel tube on the internal concrete improves the concrete's compressive strength and ductility. Moreover, the steel tube can be directly used as a formwork for the concrete during construction, thereby saving construction costs and duration.

To date, CFST has been studied extensively, due to its appreciable seismic behavior [11–14], lateral impact resistance [15], fire resistance [16–18], and post-corrosion behavior [19,20], etc. Nevertheless, fewer studies have been conducted regarding indicators of interest to stakeholders, such as life cycle economic benefits or carbon emissions reduction benefits. Furthermore, comparative assessments based on these indicators are more conducive to a comprehensive understanding of the CFST members' potential benefits and limitations. Hastak and Halpin [21] presented an evaluation framework to comprehensively consider the life cycle benefit-cost of conventional steel jackets versus carbon-composite wraps from the perspectives of structure, management, construction, and maintenance. Rossi et al. [22] investigated the life cycle environmental impacts of steel, CFST, concrete, and wood columns under the same compression-bending load design. Zhao et al. [23] conducted a life cycle assessment of multiple types of composite columns from economic and environmental perspectives. However, potential seismic risks during the life cycle have not been considered in these studies.

The suddenness and destructiveness of earthquakes may interrupt a building's functionality during its service life, especially in highly seismic regions. Additionally, it's important to note that historical major earthquakes not only cause significant economic losses but also lead to huge carbon emissions [24,25]. For example, after the 2011 Great East Japan Earthquake, the carbon emissions generated from house reconstruction alone accounted for 2.1% of Japan's carbon emissions that year [25]. Therefore, the initial cost savings and low carbon emissions don't necessarily translate into the same benefits over the building's entire life cycle incorporating seismic risks. It's crucial to thoroughly explore the trade-offs between initial investment and risk-related consequences to generate truly sustainable design solutions and make robust policies [26–33]. For instance, Zhang et al. [34] investigated and compared the life cycle economic benefits of emerging self-centering braces and conventional buckling-restrained braces considering seismic risk. Al-Attraqchi et al. [35] conducted a comparative seismic loss assessment of a rigid-frame bridge with reinforced concrete and CFST columns to demonstrate the advantages of CFST columns. Park et al. [36] developed an integrated sustainable seismic analysis model to study the relationship between carbon emissions or economic costs with seismic performance objectives. Moreover, considering the ongoing urban renewal in Europe, some recent studies [37–39] were devoted to proposing assessment frameworks aimed at identifying optimal building renovation strategies for various regions, taking into account specific climatic conditions and site hazards, with a focus on both economic and environmental impact. As far as the authors know, there have been no studies on the seismic resilience assessment of composite frame structures with CFST members based on economic and carbon emission indicators, especially its benefit comparison with typical pure steel structures, such as frame structures with HSS columns.

Based on the above, this paper presents a comparative seismic resilience assessment of the CFST frame structure and HSS frame structure, focusing on economic and environmental aspects. In the subsequent sections, the critical steps of the seismic resilience assessment methodology are first introduced, namely hazard analysis, structural analysis, damage analysis, and consequence analysis. An overview of the methods for incorporating carbon emission calculations within seismic loss assessments is also presented. Then, two comparable 9-story frame structures are designed per the Chinese design code. The resilience of these structures under four seismic hazard scenarios, classified as 50-year, 475-year, 2475-year, and 10,000-year return period, is finally evaluated based on economic and carbon emission indicators.

2. Seismic resilience assessment methodology and its integration with carbon emission calculation methods

2.1. Seismic resilience assessment methodology

The seismic resilience of a building refers to its ability to maintain and recover its original functionality after specific earthquakes. It can be evaluated quantitatively by various consequences such as repair costs, repair-induced carbon emissions, repair time, and casualties. Since the Pacific Earthquake Engineering Research (PEER) Center proposed the second generation of performance-based earthquake engineering concepts [40], seismic resilience assessment methods and associated databases have been continuously emerging, including methods like HAZUS [41], FEMA P-58 [42], REDi [43], and Chinese code GB/T 38591–2020 [44]. Despite the diversity in methods, there is a uniform underlying logic that they all adhere to, generally following the four steps of seismic hazard analysis, structural analysis, damage analysis, and loss analysis. The interrelationship of these four steps can be represented by the multiple integrals in Eq. (1).

$$\lambda(LOSS) = \iiint G(DV|DM)dG(DM|EDP)dG(EDP|IM)d\lambda(IM) \tag{1}$$

where the $\lambda(x)$ represents the probability of x. $G(x|y)$ represents the

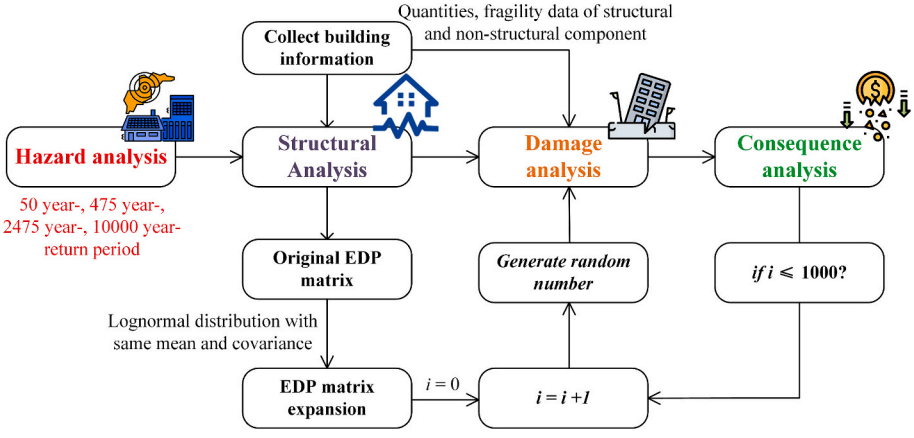

Fig. 1. The basic steps of seismic resilience evaluation.

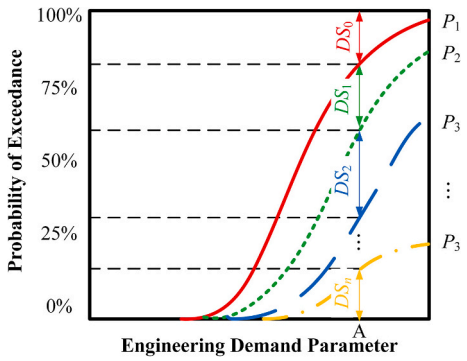

Fig. 2. Illustration of component fragility curve.

Table 1
Structural design data.

Parameter	Value
Total building area (m^2)	3375
Seismic intensity level	8
The PGA corresponds to a 475-year return period	0.20 g
Site category	II
Seismic design group	Group 2
Site characteristic period T_g (s)	0.40
Frame seismic performance level	III
Beam/wall dead load(kN/m)	6
Beam/wall live load (kN/m)	6
Floor dead load (kN/m^2)	2
Floor live load (kN/m^2)	2.5

conditional probability of x when y is given. *IM* denotes the intensity measure of earthquake events, such as peak ground acceleration *PGA* or spectral acceleration S_a, and its probability $\lambda(x)$ can reflect the site's seismic risk. *LOSS* denotes the earthquake-induced consequences, such as repair costs and repair carbon emissions estimated in this paper. *EDP* denotes the engineering demand parameter, which should be the structural response that best reflects the damage states of a specific component, so it is typically different for different types of components.

Table 2
The natural periods of the two structures.

Mode	1	2	3	4	5	6
CFST frame	2.250	2.246	2.011	0.763	0.734	0.680
HSS frame	2.233	2.224	1.989	0.766	0.735	0.681
Discrepancy	0.75%	0.98%	1.10%	0.39%	0.14%	0.15%

DM denotes the damage measure, i.e., the damage state a specific component is in. As shown in Eq. (1), the seismic risk is translated to possible consequences through multiplication with three conditional probabilities. Notably, it's impractical to derive the analytical solution of the above multiple integrals, hence the Monte Carlo simulation is commonly utilized to find its numerical solution.

According to the GB/T 38591–2020 [44], the following four basic steps (as briefly shown in Fig. 1) are taken for the comparative seismic resilience assessment:

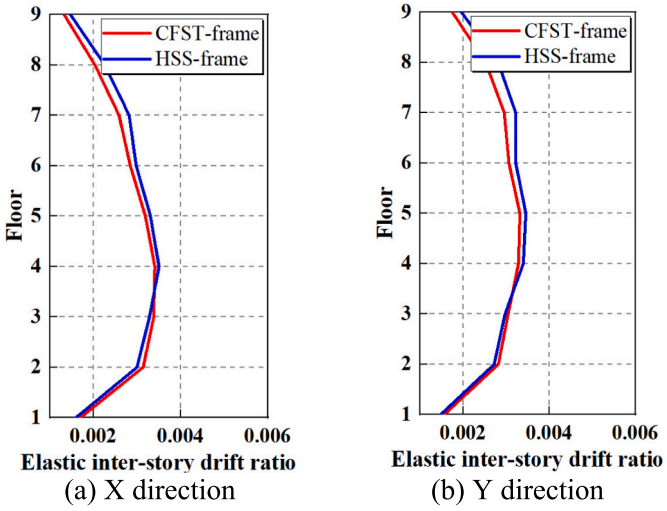

Fig. 4. Elastic inter-story drift ratio.

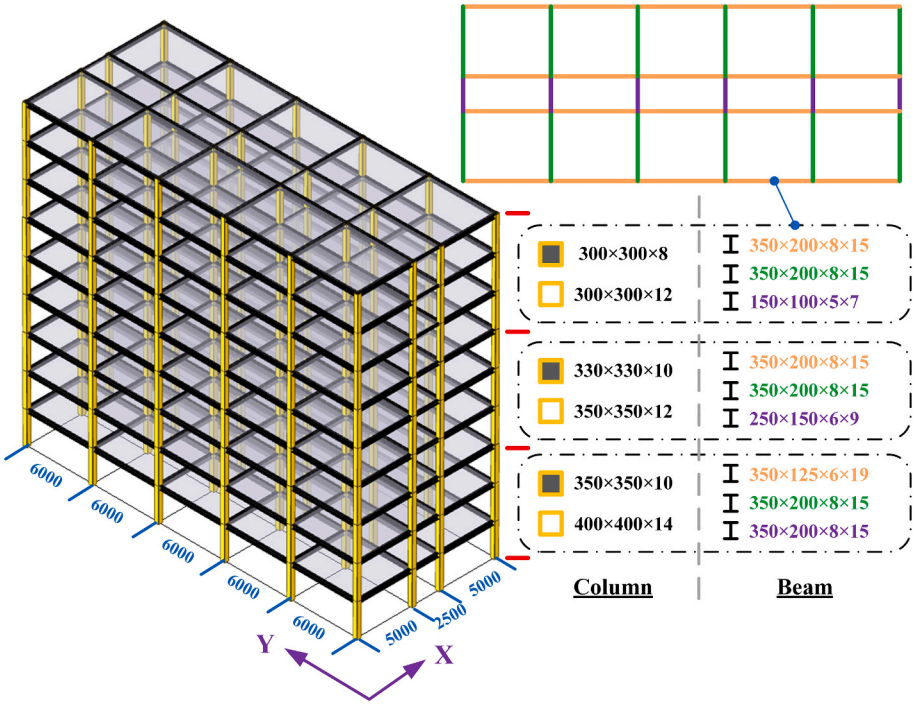

Fig. 3. The schematic of the prototype building with component size and layout information.

Table 3
Material cost and carbon emission of CFST columns and HSS columns in the two structures.

Building	Material usage		Cost (¥)	Carbon emission (kg CO_2e)
	Concrete (m^2)	Steel (ton)		
CFST frame	61.7	60.6	268,642	161,432
HSS frame	–	87.6	351,282	205,863

(1) Hazard analysis: The hazard analysis provides the seismic risk of the building site, including the IM values and corresponding occurrence probabilities. Notably, only basis (475 year-) and rare (2475 year-) levels are considered in the GB/T 38591–2020 [44] for ease of application. Hence, two more hazard levels provided in the seismic ground motion parameters zonation map of China [45], frequent (50 year-) and very rare (10,000 year-) levels, are also supplemented for a comprehensive comparative assessment. Ground motions are typically selected based on the acceleration response spectrum corresponding to the rare level. Then, the selected ground motions are scaled to different hazard levels for structural analysis. In addition to the above method, probabilistic seismic hazard analysis (PSHA) [46] and hazard-compatible ground motion selection methods (e.g., conditional spectrum method [47,48]) can also be used to perform a more refined but complex hazard analysis.

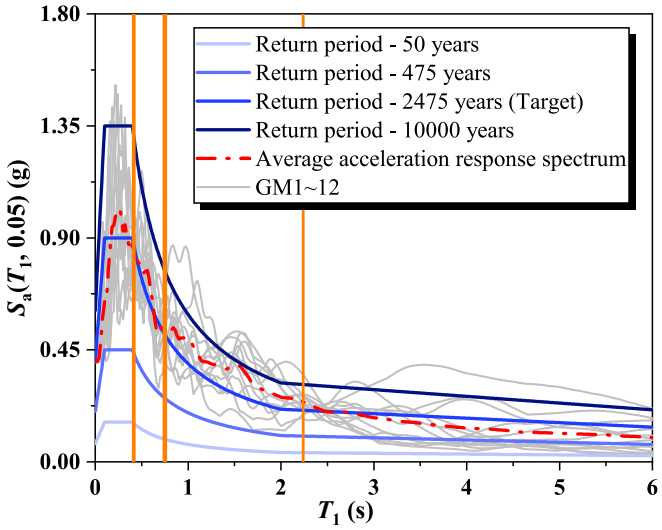

Fig. 5. The comparison of various response spectra.

(2) Structural analysis: In this step, the finite element models capable of simulating nonlinear behavior are built to obtain the structural response under seismic excitation. The obtained structural response should cover the *EDPs* required for damage analysis, such as peak floor acceleration *PFA*, peak inter-story drift ratio *PIDR*, the chord rotation of structural members θ, etc. Since the number of selected ground motions is relatively not large, the obtained *EDP* matrix needs to be expanded. The expanded *EDP* should meet the same joint lognormal distribution as the original *EDP*, namely with the same mean and deviation. The lognormal distribution of the *EDP* can be determined by Eq. (2).

$$Z = LU + M_Y \tag{2}$$

where $Z_i = [Z_1, Z_2, \ldots, Z_n]^T$, Z_i is the logarithmic value of i th EDP. L is the lower triangular matrix derived by the Cholesky decomposition of Σ_{YY}, and Σ_{YY} is the covariance matrix of the *EDP* matrix Y after taking the logarithm. $U = [U_1, U_2, \ldots, U_m]^T$, U_i is the i th independently normally distributed variable. M_Y is the mean matrix of the *EDP* matrix Y. When the matrix Σ_{YY} is full rank, m should be equal to the number of *EDP* n; when the matrix Σ_{YY} is not full rank, m should be set equal to the rank.

Table 4
Information on selected ground motions.

No.	Earthquake Name	Year	Station Name	*RSN*	*M*	*R*	V_s	*D*
1	Kocaeli_Turkey	1999	Istanbul	1164	7.51	49.66	595.2	38
2	Chi-Chi_Taiwan	1999	HWA006	1259	7.62	43.49	559.11	20.1
3	Chi-Chi_Taiwan	1999	HWA048	1294	7.62	47.35	345.89	30.5
4	Chi-Chi_Taiwan	1999	TCU042	1484	7.62	26.31	578.98	21.4
5	Chi-Chi_Taiwan	1999	TTN040	1585	7.62	43.99	728.01	35.5
6	Chi-Chi_Taiwan	1999	TTN051	1594	7.62	30.77	665.2	37
7	Hector Mine	1999	Twentynine Palms	1836	7.13	42.06	635.01	18
8	Cape Mendocino	1992	Eureka - Myrtle & West	826	7.01	40.23	337.46	20.6
9	Landers	1992	North Palm Springs	882	7.28	26.84	344.67	37.9
10	Chi-Chi_Taiwan	1999	TCU046	1486	7.62	16.74	465.55	18.4
11	Chi-Chi_Taiwan	1999	TCU122	1546	7.62	9.34	475.46	30.9
12	Denali_Alaska	2002	R109 (temp)	2111	7.9	42.99	341.56	23.1

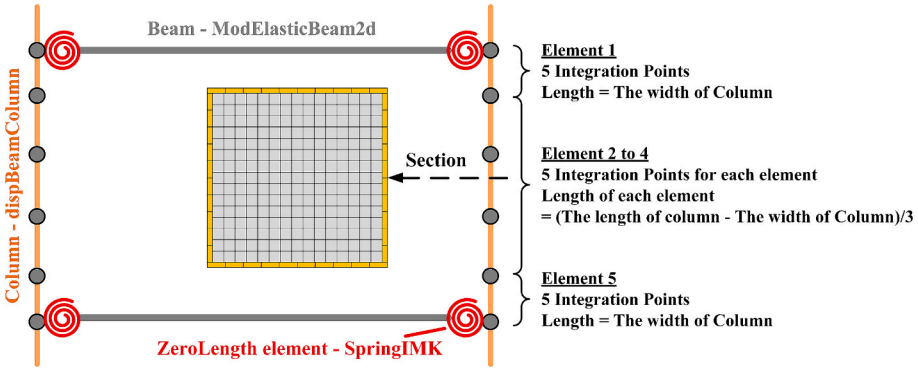

Fig. 6. The schematic diagram of the OpenSees model.

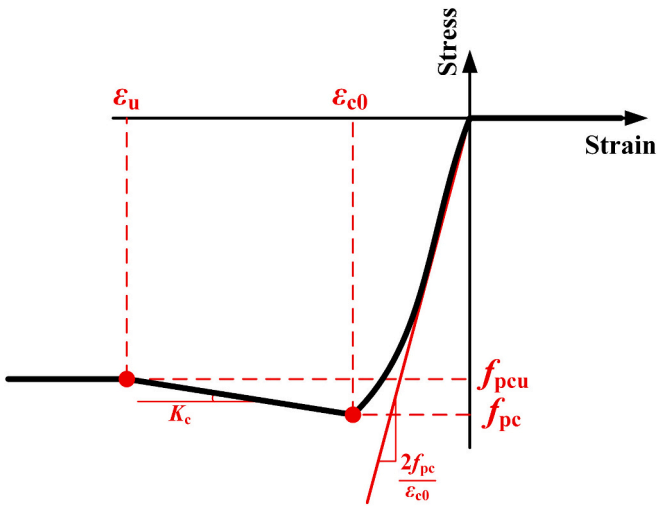

Fig. 7. The typical stress-strain relation for *Concrete01*.

(3) Damage analysis: The expanded *EDP* matrix is then utilized for Monte Carlo simulation (MCS). The number of MCS is consistent with the size of the expanded *EDP* matrix, typically >1000 times. In each MCS, the damage state of each component is determined by generating a random number and combining the probabilities of the component being in various damage states. More specifically, as shown in Fig. 2, for a given *EDP* value, the exceedance probability of the damage state i is P_i. Then, a random number R between 0 and 1 is generated. When $P_1 \leq R \leq 1$, the damage state is set to state 0; when $P_{i+1} \leq R < P_i$, the damage state is state i; when $0 \leq R < P_n$, the damage state is state n.

(4) Consequence analysis: In each MCS, the consequence of each component can be calculated by the determined damage state and consequence database. In GB/T 38591–2020 [44], two coefficients, i.e., repair coefficient and loss coefficient, are utilized to calculate the repair loss of various components, as Eq. (3). The specific values of these two coefficients for each component can be found in GB/T 38591–2020 document [44]. There is no relevant data regarding carbon emissions provided in the seismic evaluation code. The estimation of repair-related carbon emissions is based on the "repair-cost ratio" method and China's localized carbon emission factors, which will be detailed in Section 2.2.

$$\text{Repair Loss} = \text{Repair coefficient} \times \text{Loss coefficient} \times \text{Component Cost} \tag{3}$$

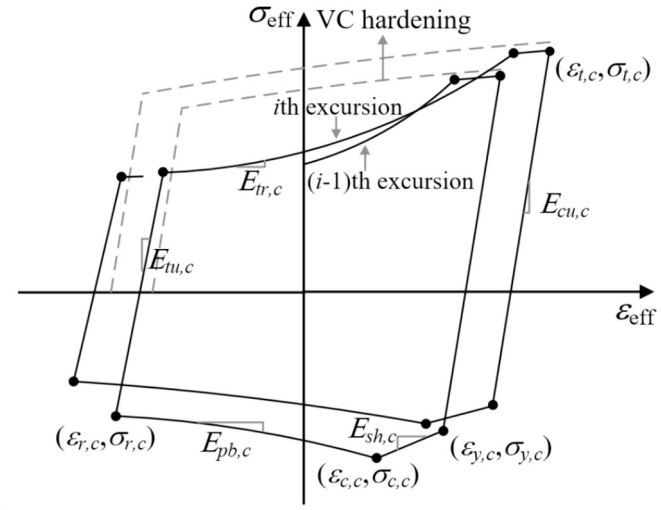

Fig. 8. The constitutive relationship of *CFSTsteel* uniaxial material model.

2.2. Overview of approaches for integrating loss estimation and carbon emissions calculation

Generally, three methods can be utilized to calculate the building-related carbon emissions [49], namely process-based life cycle assessment (Process-LCA), economic input output-life cycle assessment (EIO-LCA), and carbon emission factor. The concepts of these three methods are as follows:

(1) Process LCA is an approach used to evaluate the environmental impacts of a product, process, or activity throughout its entire life cycle. This includes the extraction of raw materials, manufacturing, distribution, use, and disposal. The assessment accounts for all relevant inputs and outputs, including energy, materials, and emissions to air, water, and soil. Thus, the Process LCA offers a detailed and precise assessment of a product's environmental impact, but it often requires extensive data collection and can be complex and time-consuming.

(2) EIO-LCA is a method that combines life cycle assessment with economic input-output analysis to estimate the environmental impacts of final demand for products and services within a national economy. It uses a comprehensive, economy-wide model that links industries through their supply chains and accounts for all the economic transactions that occur between them. By doing

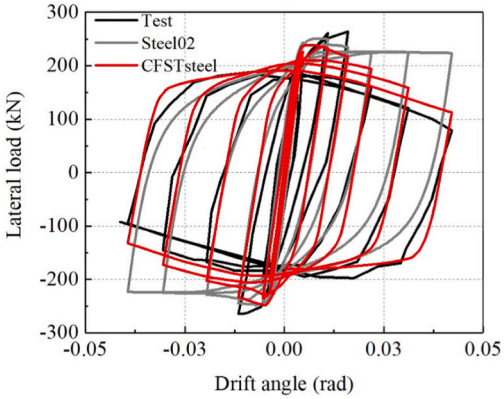

(a) CFST column (Inai et al. [74])

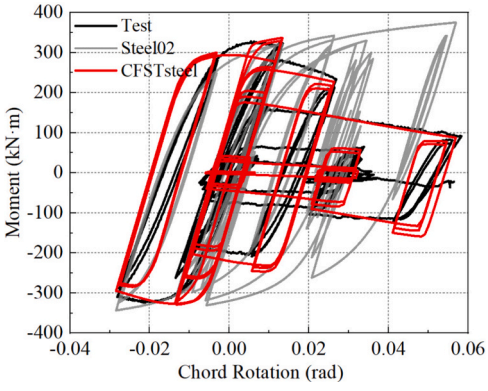

(b) HSS column (Suzuki et al. [75])

Fig. 9. Feasibility verification of the modeling method for columns.

so, EIO-LCA can estimate the environmental impacts associated with the production and consumption of goods and services, including indirect effects along the supply chain. EIO-LCA provides a quick and cost-effective way to estimate the broad environmental impacts of economic activities, yet it may lack the specificity to differentiate between products within the same sector.

(3) The carbon emission factor is a coefficient that corresponds to activity level data on carbon emissions. It is used to quantify the carbon emissions per unit activity level data. The activity level data is quantitative data that reflects greenhouse gas emissions caused by human activities. Compared with the EIO-LCA method, the carbon emission factor can distinguish differences between different products within the same sector, such as the difference between concrete products of different grades. However, it is not as refined as the Process LCA method. Therefore, the carbon emission factor is a practical and standardized tool for estimating emissions, recommended by the IPCC, and has been used in several Chinese carbon emission calculation codes or guidelines [50–52].

As summarized in a review of the integration of seismic loss

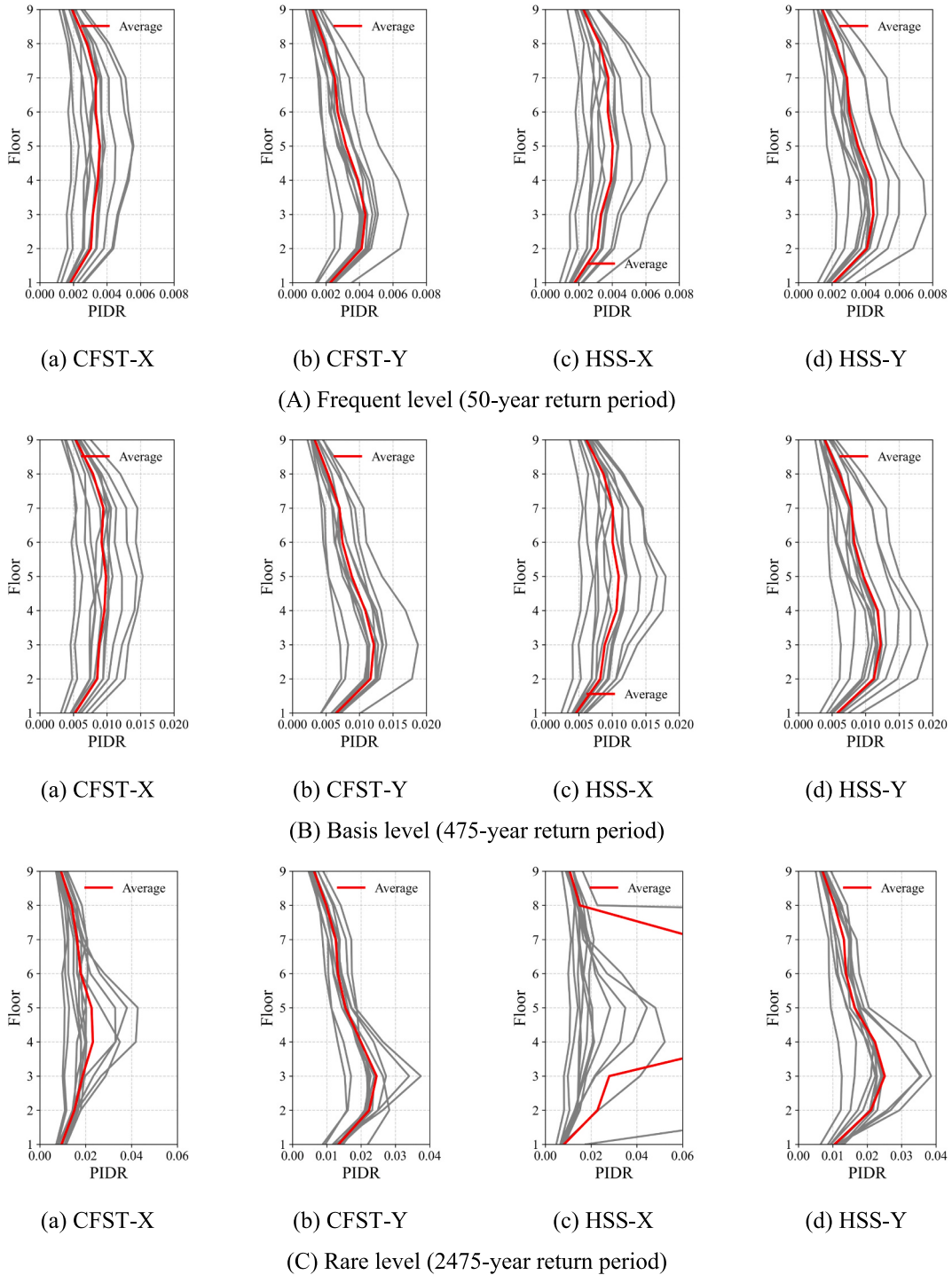

Fig. 10. The PIDR results of the two structures under four hazard levels.

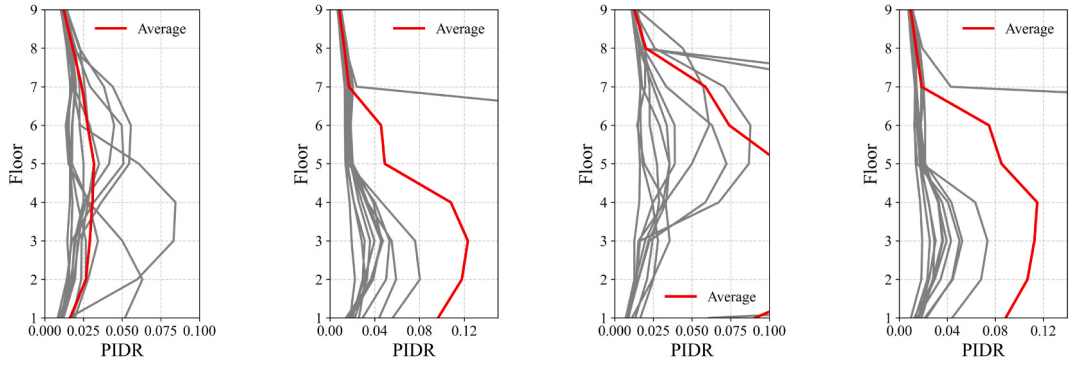

(a) CFST-X (b) CFST-Y (c) HSS-X (d) HSS-Y

(D) Very rare level (10000-year return period)

Fig. 10. (*continued*).

Table 5
The cost and carbon emission factor of considered components.

Component	EDP	Quantity			Floor	Unit	Cost (¥/unit)	Carbon emission factor ($kgCO_2e$/unit)
		X	Y	No direction				
H-shaped steel beams	θ	15 beams	20 beams		1–9	ton	3870	2350 [50]
Square steel tube	θ			20 columns	1–9	ton	4010	2350 [50]
Concrete-filled square steel tube	θ			20 columns	1–9	ton (steel); m^3 (concrete)	4010 (steel); 415 (concrete)	2350 (steel); [50] 308 (concrete) [50]
Glass curtain wall	PIDR	112.5	112.5		1–9	m^3	1520	254 [51]
Interior partition wall (steel furring with gypsum board)	PIDR	37.5	37.5		1–9	m^3	220	87 [51]
Partition wall finishes (gypsum board)	PIDR	2.835	2.835		1–9	m^3	130	9.6 [51]
Suspended ceiling (steel furring with gypsum board)	PFA			337.5	1–9	m^3	225	38 [51]
Suspended light	PFA			5.625	1–9	Each	200	7.92 [77]
Hot pipe (polypropylene-random pipe)	PFA			52.125	1–9	m	60	0.7 [52]
Sewage pipe (cast iron)	PFA			21.375	1–9	m	260	141 [52]
HVAC ducts (galvanized steel tube)	PFA			35.625	1–9	Each	40	19 [52]
HVAC drops/diffusers (galvanized steel tube)	PFA			3.375	1–9	Each	150	72 [52]
Fire sprinkler water pipe (plastic coated seamless welded steel pipe)	PFA			75	1–9	m	165	23 [52]
Nozzle riser (plastic coated seamless welded steel pipe)	PFA			3.375	1–9	Each	68	10 [52]
Elevator	PFA			1	1	Each	200,000	15,416 [77]
Variable air volume box	PFA			2.625	1–9	Each	800	384
Chiller	PFA			1	9	Each	125,000	16,894 [77]
Cooling tower	PFA			1	9	Each	55,000	7433
Air handling unit	PFA			1	9	Each	43,632	5897
Motor control centre	PFA			1	9	Each	5342	722

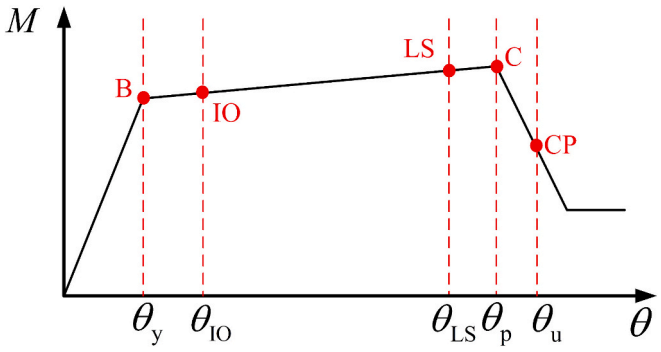

Fig. 11. The typical moment (M) – chord rotation (θ) relation of steel members.

estimation and life cycle assessment [49], three methods are typically used for translating the damages and associated repairs into carbon emissions, which are listed as follows:(1) Directly utilize the EIO-LCA method to transform the results of economic loss estimation [53,54]; (2) Utilize repair-cost ratios and the components' carbon emissions from pre-use stage [55–57]; (3) Utilize repair descriptions and any carbon emission calculation method [58–61].

It is worth noting that the choice of method mainly depends on the richness of information available. When known information is very limited, for example, there is even no specific information about the component, approach (1) can be used. Approach (3) can be used when a detailed description of the repair of each component is known, i.e., the labor, machinery, and materials used in the repair process. In FEMA P-58, approach (3) is used and combined with the EIO-LCA database proposed by Carnegie Mellon University to calculate the repair-related

Table 6
The fragility data and consequence data about the steel members.

Component type		Chord rotation (θ)				
		θ_y		θ_{IO}	θ_{LS}	θ_u
H-shaped steel beam	$\frac{b_f}{2t_f} \le \frac{9}{\sqrt{f_y/235}} and \frac{h}{t_w} \le \frac{72}{\sqrt{f_y/235}}$	$\theta_y = Wf_{ye}l_b/6EI_b$		2	10	12
	$\frac{b_f}{2t_f} \ge \frac{11}{\sqrt{f_y/235}} or \frac{h}{t_w} \ge \frac{110}{\sqrt{f_y/235}}$			1.25	4	5
	other			Linear interpolation		
	Damage state	DS0 $\theta \le \theta_y$	DS1 $\theta_y < \theta \le \theta_{IO}$	DS2 $\theta_{IO} < \theta \le \theta_{LS}$	DS3 $\theta_{LS} < \theta \le \theta_u$	DS4 $\theta \ge \theta_u$
	Loss coefficient	0	0.10	0.35	0.65	1.00
	Repair coefficient	0	1.10	1.72	1.72	1.72
Square steel tube column	$\frac{P}{P_{CL}} < 0.2$	$\frac{b_f}{2t_f} \le \frac{19}{\sqrt{f_y/235}} and \frac{h}{t_w} \le \frac{51}{\sqrt{f_y/235}}$	$\theta_y = \left(1 - \frac{P}{P_{CL}}\right) Wf_{ye}l_c/6EI_c$	2	10	12
		$\frac{b_f}{2t_f} \ge \frac{33}{\sqrt{f_y/235}} or \frac{h}{t_w} \ge \frac{79}{\sqrt{f_y/235}}$		1.25	4	5
		other		Linear interpolation		
	$\frac{P}{P_{CL}} \ge 0.2$	$\frac{b_f}{2t_f} \le \frac{19}{\sqrt{f_y/235}} and \frac{h}{t_w} \le \frac{45}{\sqrt{f_y/235}}$		1.25	$15 - 23.3\frac{P}{P_{CL}}$	$15 - 23.3\frac{P}{P_{CL}}$
		$\frac{b_f}{2t_f} \ge \frac{33}{\sqrt{f_y/235}} or \frac{h}{t_w} \ge \frac{68}{\sqrt{f_y/235}}$		1.25	1.5	1.8
		other		Linear interpolation		
	Damage state	DS0 $\theta \le \theta_y$	DS1 $\theta_y < \theta \le \theta_{IO}$	DS2 $\theta_{IO} < \theta \le \theta_{LS}$	DS3 $\theta_{LS} < \theta \le \theta_u$	DS4 $\theta \ge \theta_u$
	Loss coefficient	0	0.10	0.35	0.65	1.00
	Repair coefficient	0	1.22	4.50	4.50	4.50

l_b is the length of beam; l_c is the length of column; E is the material elastic modulus; W is the plastic modulus for the cross section; f_y is the design yield strength of steel; f_{ye} is the expected yield strength of steel; b_f is the width of the beam flange; t_f is the thickness of the beam flange; h is the height of the beam; t_w is the thickness of the beam web; I_b, I_c are the moment of inertia of steel beam section and column section, respectively; P is the column axial force; P_{CL} is the column axial compressive capacity; Linear interpolation is performed based on the flange width-thickness ratio and web height-thickness ratio, and the smaller value is taken.

Table 7
The fragility data and consequence data about the CFST columns.

Component type	Chord rotation (θ)			
	θ_y	θ_p		θ_u
Square concrete-filled steel tubular column	$K_a = 24K_e/L^3$ $K_e = E_sI_s + 0.2E_cI_c$ $P_y = \begin{cases} 2(2.5n^2 - 0.75n + 1)M_y/L\ (0 \le n \le 0.4) \\ 2(0.63n + 0.848)M_y/L\ (0.4 < n < 1) \end{cases}$ $n = \frac{P}{P_{CL}}$ $\begin{cases} n + a\cdot\left(\frac{M_y}{M_u}\right) = 1 \\ -b\cdot n^2 - c\cdot n + \frac{M_y}{M_u} = 1 \end{cases}, \begin{cases} a = 1 - 2\eta_0 \\ b = \frac{1 - \zeta_0}{\eta_0^2} \\ c = \frac{2\cdot(\zeta_0 - 1)}{\eta_0} \end{cases}$ $\zeta_0 = 1 + 0.14\xi^{-1.3}$ $\eta_0 = \begin{cases} 0.5 - 0.318\xi\ (\xi \le 0.4) \\ 0.1 + 0.13\xi^{-0.81}\ (\xi > 0.4) \end{cases}$ $M_u = \gamma_m\cdot W_{scm}\cdot f_{scy}$ $\gamma_m = 1.04 + 0.48ln(\xi + 0.1)$ $W_{scm} = B^3/6$ $f_{scy} = (1.18 + 0.85\xi)\cdot f_{ck}$ $\theta_y = \frac{P_y}{K_aL}$	$\theta_p = (1.7 + n + 0.5\xi)\cdot\theta_y$		$\lambda = 2\sqrt{3}L/B$ $K_d = \frac{-9.83\cdot n^{1.2}\cdot\lambda^{0.75}\cdot f_y}{E_s\cdot\xi}\cdot K_a$ $\theta_u = \theta_p - 0.15\cdot\frac{P_y}{K_d\cdot L}$
Damage State	DS0 $\theta \le \theta_y$	DS1 $\theta_y < \theta \le \theta_p$	DS2 $\theta_p < \theta \le \theta_u$	DS3 $\theta \ge \theta_u$
Loss coefficient	0	0.10	0.50	1.00
Repair coefficient	0	1.22	4.50	4.50

K_a and K_d are the initial elastic stiffness and descending stiffness in the lateral load versus lateral displacement hysteretic relationship of CFST columns, respectively; K_e is the elastic stiffness of the composite cross section; E_s and E_c are the elastic modulus of steel and concrete, respectively; P_y is the CFST column axial yield capacity; M_y is the column yield moment; M_u is the moment capacity; n is the axial load level; ξ is the constraining factor; λ is the slenderness ratio; W_{scm} is the flexural rigid; f_{scy} is the compressive strength index; f_{ck} is the characteristic concrete strength; L is the effective buckling length of the column in the plane of bending; B is the width of rectangular steel tube; other undefined parameters, such as a, b, c, can be treated as fitted coefficients. A more detailed explanation of all the above parameters can be found in Ref. [11].

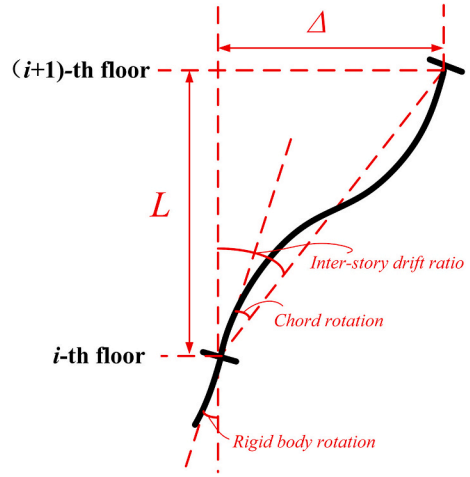

Fig. 12. The schematic diagram of the calculation of a column's chord rotation.

carbon emissions. However, the GB/T 38591–2020 used in this paper does not provide detailed repair descriptions, but provides the repair-cost ratios, which are naturally consistent with the use of approach (2). Thus, the "repair-cost ratio" method and China's localized carbon emission factors are used to estimate the repair-related carbon emissions in this paper.

3. Investigated square CFST and HSS column-based frame structures

Two code-compliant 9-story frame structures were designed by design software YJK [62] according to Chinese design code: one is a composite frame structure with H-shaped steel beams and CFST columns (CFST frame), and the other is a pure steel frame structure with H-shaped steel beams and HSS columns (HSS frame). The building is assumed to be in Beijing. The detailed structural design data is presented in Table 1. The C40 concrete (the cubic standard compressive strength is 40 MPa) and Q355 steel (the yield strength is 355 MPa) are used for structural components. The height of all floors is set to 3.0 m. The planar and elevation grids of the two structures, as well as the detailed section dimensions of each structural member can be found in Fig. 3.

Since the paper focuses on the differences brought by CFST columns and HSS columns, the steel beams of the two structures are designed to be the same. Besides, the peak value and distribution of elastic inter-story drift ratio and the main natural periods of the two structures are designed to be consistent to ensure the comparability of their seismic designs, as presented in Table 2 and Fig. 4. Notably, since standard section steel dimensions were selected for all members, it may be unrealistic to have the complete same design response for both structures. Compared with HSS columns, a smaller steel tube cross-section can be selected when using CFST columns.

Given that the two structures differ only in column type and size, a comparison can be made by calculating the carbon emissions and economic differences resulting from these variations. Differences in connection detail and construction aspects due to column differences are disregarded. The cost and carbon emissions are determined by multiplying the price or carbon emission factor by the quantity of material used for the columns. As of April 2024, the prices of square steel tubes and C40 concrete in Beijing's building material market are ¥4010 per ton and ¥415 per cubic meter, respectively. According to the Chinese standard for building carbon emission calculation (GB/T51366-2019) [50], the carbon emission factors for steel and concrete are 2350 kgCO2e per ton and 308 kgCO2e per cubic meter, respectively. Table 3 presents a comparison of the costs and carbon emissions of the materials used in the two types of structural columns. In the case studied, the cost of CFST columns is 76.5% of that of HSS columns, while the carbon emissions are 78.4%, indicating significant economic and carbon reduction benefits.

4. Comparative study based on economic and carbon emission indicators

4.1. Seismic hazard analysis and ground motion selection

As mentioned before, four hazard levels with different return periods, namely basis (50-year), frequent (475-year), rare (2475-year), and very rare (10000-year), are considered in the comparative assessment. Strong ground motions are selected from the PEER NGA West 2 database. Initial screening with the following criteria [44,63]: (1) Moment magnitude (M): larger than 7; (2) Epicentral distance (R): [9 km, 52 km]; (3) Shear wave velocity (V_s): larger than 260 km/s; (4) Effective duration (D): larger than 15 s. Then, a total of 12 records were selected. The average response spectrum of these records is statistically consistent with the rare-level target spectrum, that is, their error at the main natural periods of the structures is <20%, which meets the GB/T 38591–2020, as shown in Fig. 5. The information on selected ground motions is presented in Table 4.

4.2. Structural analysis

The two-dimensional planar models of each structure in both directions were created separately in OpenSees [64]. In each direction of the structure, half the number of frames is modeled independently, and then the horizontal degrees of freedom of each node at each floor are constrained based on the "rigid diagram assumption".

Based on the physical experimental results of CFST and HSS columns, the local buckling is the dominant failure mode that could lead to the cyclic deterioration of strength and stiffness. Therefore, it is crucial that such phenomenon be accurately captured by the numerical models. Modeling methods capable of simulating the deterioration of structural members can be categorized into three types: (1) continuum finite element (CFE) method, (2) concentrated plastic hinge model, and (3) distributed plastic model (fiber-based model). The first method is the most accurate and can effectively simulate the physical phenomena of buckling behavior. However, it comes with a high computational cost, making it challenging to apply to nonlinear time history analyses of structural systems. The second method is widely used in earthquake engineering due to its computational efficiency. Nevertheless, it struggles to capture the coupling effects of axial and bending loads, which is crucial for considering the fluctuation in axial forces experienced by columns under seismic excitation. In contrast, the third method offers acceptable computational efficiency and can account for the coupling effects of axial and bi-directional bending, giving it a significant advantage in modeling lateral-resistant members, such as columns. The fiber-based model requires the cross-section of a structural member to be divided into multiple fibers, with each fiber assigned a corresponding uniaxial material model. Thus, the columns were constructed by utilizing a fiber-based model, and the beams were constructed by using a concentrated plastic hinge model, as shown in Fig. 6.

More specifically, each beam was constructed by an equivalent combination of one elastic element with stiffness-proportional damping and two springs at its two ends with no stiffness-proportional damping. The spring is a *ZeroLength* element with the modified Ibarra-Medina-Krawinkler deterioration model (i.e., *IMKBilin* in OpenSees) [65] to capture the beams' deterioration behavior under seismic excitation. The parameters of the *IMKBilin* model were calculated according to Ref. [66], and the contribution of slab restraint on the beam was also considered based on Ref. [67].

For the CFST columns, the infilled concrete was constructed by using a zero tensile strength material *Concrete01*. The *Concrete01* material model has four key input parameters, i.e., compressive strength at 28 days f_{pc}, strain at maximum strength ε_{c0}, crushing strength f_{pcu}, strain at crushing strength ε_u, as shown in Fig. 7. The f_{pc} was calculated by the Eq.

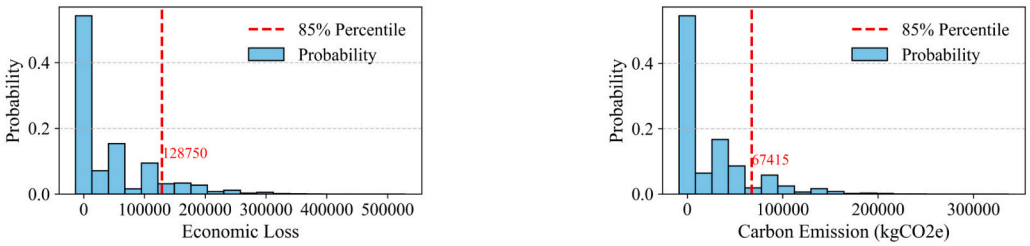

(a) CFST - Economic loss (b) CFST - Carbon emission

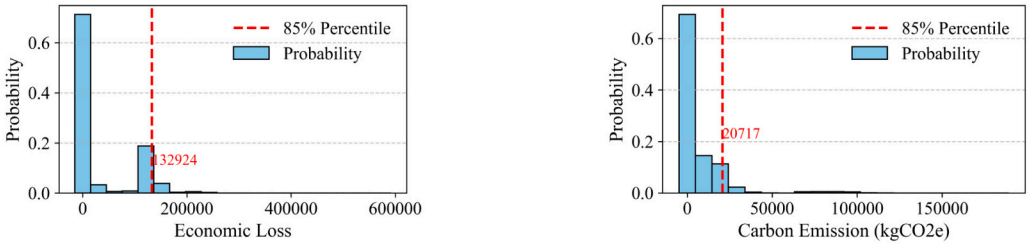

(c) HSS – Economic loss (d) HSS – Carbon emission

(A) Frequent level (50-year return period)

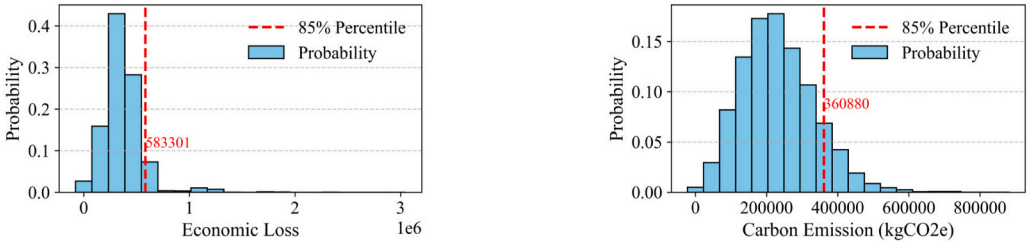

(a) CFST - Economic loss (b) CFST - Carbon emission

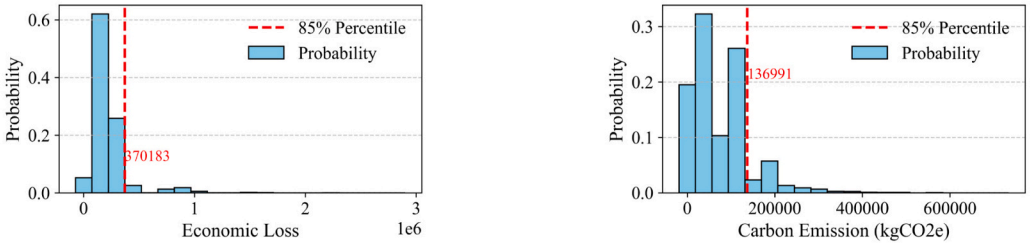

(c) HSS – Economic loss (d) HSS – Carbon emission

(B) Basis level (475-year return period)

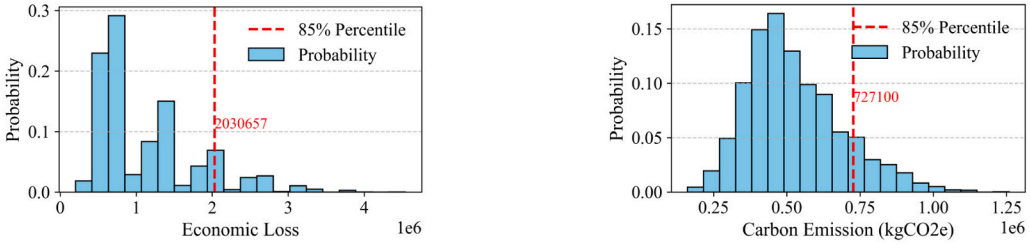

(a) CFST - Economic loss (b) CFST - Carbon emission

Fig. 13. Comparison of the economic loss and repair-related carbon emission of the two structures under four hazard levels.

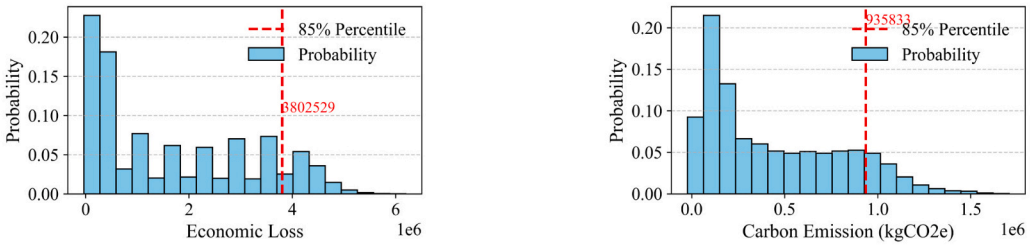

(c) HSS – Economic loss (d) HSS – Carbon emission

(C) Rare level (2475-year return period)

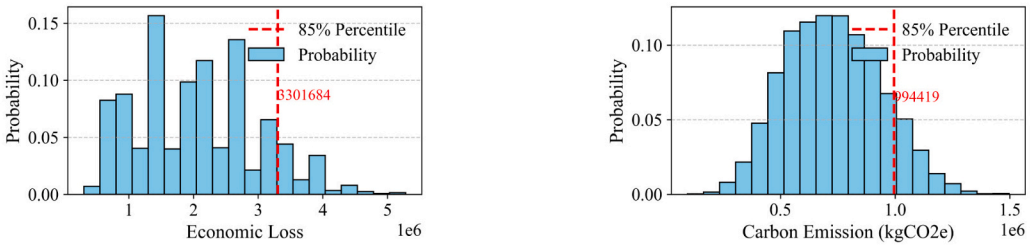

(a) CFST - Economic loss (b) CFST - Carbon emission

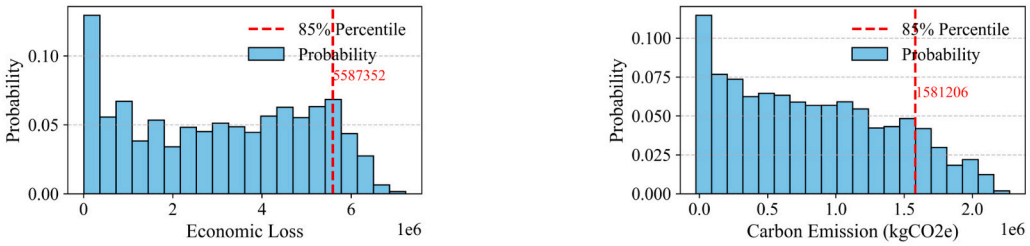

(c) HSS – Economic loss (d) HSS – Carbon emission

(D) Very rare level (10000-year return period)

Fig. 13. (*continued*).

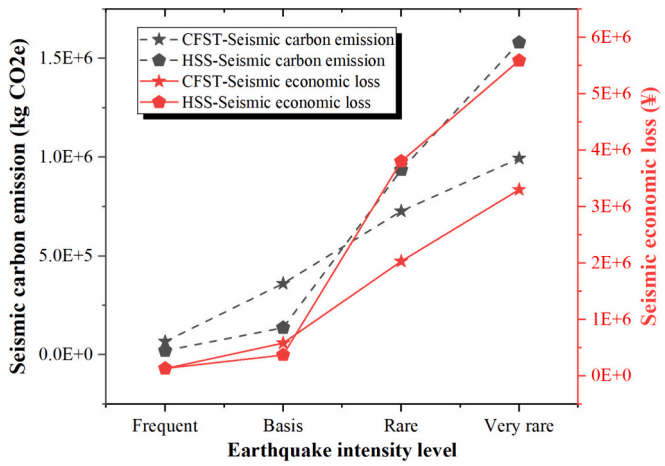

Fig. 14. Comparison of the 85th percentile consequences under four earthquake intensity levels.

(4) and (5) proposed by Han et al. [68].

$$f_{pc} = \left[1 + \left(-0.0135\cdot\xi^2 + 0.1\cdot\xi\right)\cdot\left(\frac{24}{f_c'}\right)^{0.45}\right]\cdot f_c' \tag{4}$$

$$\xi = \frac{A_s\cdot f_y}{A_c\cdot f_{ck}} \tag{5}$$

where f_c' is the cylinder compressive strength, which equals 0.83 times of the cubic compressive strength f_{cu}; ξ is the confinement factor for the confined core concrete; A_s is the cross-sectional area of steel; A_c is the cross-sectional area of concrete; f_y is the yield strength of steel. The elastic modulus of concrete E_c was set as $4700\sqrt{f_c'}$(MPa). The ε_{c0} was then calculated by Eq. (6) [69], and the crushing strength and strain were determined by Eq. (7)-(9) [70].

$$\varepsilon_{c0} = \frac{2f_{pc}}{E_c} \tag{6}$$

$$K_c = -332.75\cdot R\cdot f_{pc} + 9.60\cdot f_{pc} \tag{7}$$

$$\frac{f_{pcu}}{f_{pc}} = 0.32\cdot R^{-0.5} \tag{8}$$

$$R = (B/t)\cdot\sqrt{f_y/E_s}\cdot f_{pc}/f_y \tag{9}$$

where K_c is the slope of the descending branch shown in Fig. 7, the B is the width of the square section.

The *CFSTsteel* uniaxial material model proposed by Wang et al. [71] is adopted to capture the local buckling of CFST and HSS members under cyclic loads. The constitutive relationship of *CFSTsteel* model is shown in

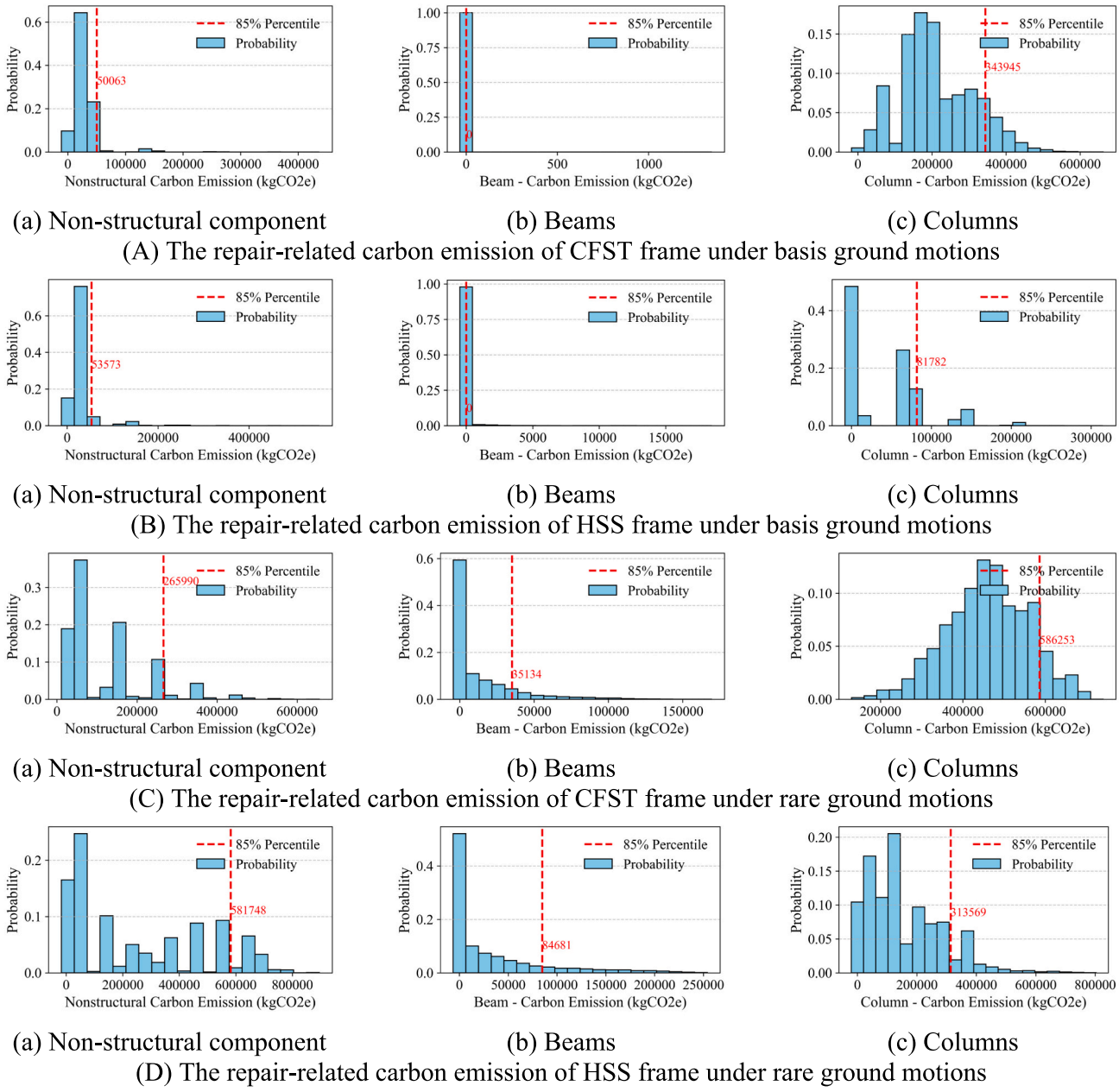

Fig. 15. Comparison of the repair-related carbon emission of non-structural components, beams, columns under basis and rare ground motions.

Fig. 8. Prior to the onset of local buckling on the steel tube, the effective stress-strain relation is described within the framework of rate-independent J_2 plasticity. The Voce-Chaboche (VC) model [72] is employed to simulate the combined isotropic and kinematic hardening of steel. After the local buckling occurred at the steel tube, the post-buckling and tensile reloading behavior is described using an exponential function. Cyclic deterioration of strength and stiffness is traced via a well-established energy-based deterioration rule, which is proposed by Rahnama and Krawinkler [73]. When the steel plate undergoes local buckling recovery and is stretched to a new tensile strain history, the effective stress-strain relation exhibits VC hardening property. Despite the differences in local buckling modes between CFST and HSS members, the local response of the steel tube could be described within the proposed *CFSTsteel* model framework [71]. It should be noted that the input parameters for CFST and HSS are different, due to the influence of the infilled concrete on the buckling mode of the outside steel tube. The proposed uniaxial material model named *CFSTsteel* has been implemented in the Open System for Earthquake Engineering Simulation (OpenSees) platform. This model is available for user access via: https://opensees.github.io/OpenSeesDocumentation/.

To assess the feasibility of the column modeling approach, simulations were performed based on two horizontal hysteretic loading tests from the literature: one involving a CFST column [74] and the other an HSS column [75]. The results of these simulations, including comparisons with the experimental data, are presented in Fig. 9. The *Steel02* material model, which is an isotropic hardening model, was utilized and compared with the *CFSTsteel* adopted in this study. It can be observed that the *CFSTsteel* can capture the degradation behavior of the components more effectively than the *Steel02* model, thus providing a closer fit to the experimental results, especially for the HSS column. Utilizing the *Steel02* model in structural analyses, particularly under strong ground motions with high hazard levels, might lead to an overestimation of the structure's performance.

Then, the above modeling strategy was used to construct both the

composite structure and the steel structure. The Rayleigh damping was adopted and determined by the first two natural periods. According to the GB/T 38591–2020, the damping ratio of the CFST frame was set to 0.05 under all earthquake scenarios, while the damping ratio of the HSS frame was set to 0.04 under frequent and basis earthquakes, and 0.05 under rare and very rare earthquakes. The PIDR results of the time history analyses under four hazard levels are presented in Fig. 10. It can be observed that under the frequent and basis ground motions, the mean PIDR curves of the two structures are relatively consistent. The response of the HSS frame is slightly larger than that of the CFST frame, which may be due to the minor differences as shown in Fig. 4. In addition, the damping ratio of the HSS frame is smaller than that of the CFST frame, that is, the energy dissipation capacity is relatively weaker, which may also lead to a larger response under certain ground motions. Under the rare level and very rare level ground motions, the advantage of CFST is demonstrated. For the CFST frame, the presence of infilled concrete improves the local buckling prevention ability of the external steel tube, making its collapse probability smaller than that of the HSS frame.

4.3. Damage analysis and consequence analysis

Table 5 presents the cost and carbon emission factor of considered components used for damage and consequence analysis. The material usage of structural components can be estimated according to the structural layout and specific dimensions presented in Fig. 3, without considering the material consumption of connections (welded or bolted connections, etc.). The quantity and cost of non-structural components were estimated by the "Standardized Quantity Estimation Tool" and the website online tool [76] provided by the GB/T 38591–2020 [44], respectively. The cost of steel and concrete was adopted from the prices in building material markets in Beijing, China in April 2024. The carbon emission factors of most components were referenced from several Chinese building carbo emission calculation guidelines and databases [50–52,77]. Carbon emission factors for some HVAC-related components are not available, i.e., the variable air volume box, cooling tower, air handling unit, and motor control center. Considering that they belong to the same industry sector, their carbon emission factors are estimated proportionally based on their costs and the cost of products in the same sector with known carbon emission factors (i.e., chiller).

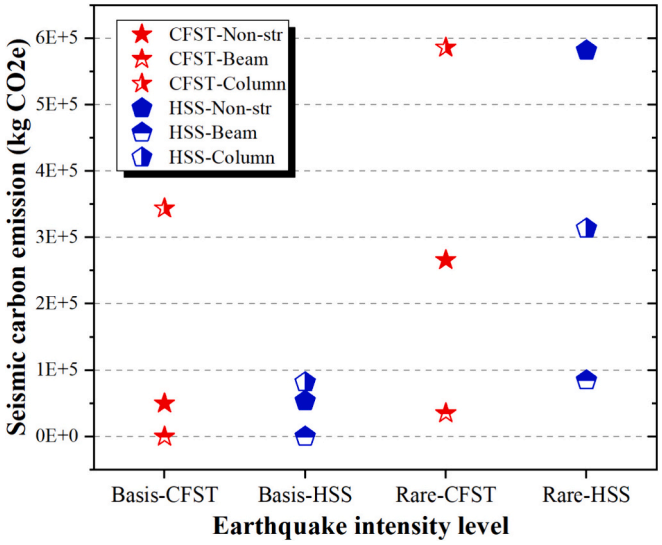

Fig. 16. Comparison of the 85th percentile carbon emission of non-structural components, beams, columns under basis and rare ground motions.

The fragility functions of H-shaped steel beams, square steel tube columns, and non-structural components can be found in the GB/T 38591–2020 document. The damage states of the steel beams and columns are generally determined by the maximum chord rotation obtained from the time history. The typical moment (M)-chord rotation (θ) relation of steel members is presented in Fig. 11.

θ_y, θ_{IO}, θ_{LS}, θ_p, θ_u are the chord rotations at the nominal yield point B, performance point IO, performance point LS, peak point C, and ultimate point CP. Table 6 presents the fragility data and consequence data about the steel members. The M-θ relation of the square CFST column is not provided in GB/T 38591–2020, and then was adopted from Ref. [11], as shown in Table 7. The loss coefficient and repair coefficient of the damaged CFST column were assumed to be similar to the steel tube column.

For beams, the rotation angle of the plastic hinge element was used as the chord rotation angle. For columns, the chord rotation angle was taken as the inter-story drift ratio minus the rotation angle of the column bottom node (the floors below drive the upper part to generate rigid body rotation), as shown in Fig. 12. The larger values of the structure's responses in the two directions were used for the determination of non-directional components' damage states.

Figure 13 presents the comparison of the economic loss and repair-related carbon emission of the two structures under four hazard levels. The 85th percentile of the consequence was taken as the comparison indicator, as further shown in Fig. 14. Under the frequent and basis ground motions, although the response of the CFST frame was found to be relatively smaller during previous structural analysis, its seismic consequences are larger than HSS frame. This outcome is because the characteristic rotation angles of the CFST columns, calculated in Table 7, are significantly smaller than those of the steel tube columns calculated in Table 6. This indicates that while the presence of concrete improves the local buckling prevention ability of the external steel tube, it also reduces the ductility of the member. Consequently, when subjected to the same rotation angles, the repair consequences of CFST columns are greater. Under rare and very rare ground motions, the losses caused by non-structural elements dominate, and in such cases, the HSS frame with higher structural response and collapse probability results in greater seismic loss.

Moreover, it is observed that the differences between the two structures in terms of economic and carbon emission indicators are not necessarily consistent, due to the diversity caused by varying economic costs and carbon emission proportions of different components and the varying consequences of each component under different earthquake scenarios. For instance, under the frequent and basis level, the HSS

Table 8
The life cycle seismic consequence of the two structures. (The building service life is set to 50 years).

Hazard level (Return period)	Exceedance probability in 50 years	Occurrence probability in 50 years	Economic (¥)		Carbon emission (kg CO_2e)	
			CFST	HSS	CFST	HSS
Frequent (50-year)	63%	53%	128,750	132,924	67,415	20,717
Basis (475-year)	10%	8%	583,301	370,183	360,880	136,991
Rare (2475-year)	2%	1.5%	2,030,657	3,802,529	727,100	935,833
Very rare (10000-year)	0.5%	0.5%	3,301,684	5,587,352	994,419	1,581,206
	Life cycle seismic consequence		161,854	185,017	80,475	43,874
	Initial cost and carbon emission		268,642	351,282	161,432	205,863
	Total		430,496	536,299	241,907	249,737

frame is similar to the CFST frame in terms of economic indicators but has a significant advantage in terms of carbon emission indicators.

The comparative results presented in Figs. 15 and 16, which show the significant consequences of CFST columns under basic earthquakes and the predominant impact of non-structural elements under rare earthquakes, confirm the aforementioned observations. However, it is noteworthy that, considering the significant differences in ductility between the two types of columns calculated in Table 6 and Table 7 and their considerable impact on the results, a comparative study and detailed examination of the full-range capacity of these components should be further investigated in the future.

Furthermore, by incorporating the exceedance probabilities of different hazard levels and the 85th percentile indicators, the life cycle seismic consequences are calculated, as shown in Table 8. It can be seen that the results obtained for the two structures in terms of economic and carbon emission indicators are opposite. From the perspective of life cycle seismic consequences, the CFST frame is superior to the HSS frame in economic indicators but inferior in carbon emission indicators. When further considering the initial costs and carbon emissions of structural columns (Table 3), the CFST frame then has advantages in both indicators.

5. Summary and conclusions

This paper presents a comparative seismic resilience assessment of CFST columns-frame structure and HSS columns-frame structure based on economic and carbon emission indicators. Two comparable code-compliant 9-story frame structures were designed and used for the comparative study: one is a H-shaped steel beams-CFST columns composite frame structure, and the other is a H-shaped steel beams-HSS columns pure steel frame structure. Four seismic hazard scenarios were then considered. In structural analysis, a fiber-based uniaxial material model with softening, validated by experimental data, was employed to simulate the steel tubes to capture the possible nonlinear local buckling behavior under earthquake exactions. In consequence analysis, the damage-induced economic loss data was sourced from GB/T 38591–2020, and the damage-induced carbon emission data was estimated based on "repair-cost ratios" and China's localized carbon emission factors. The main conclusions and comments are summarized as follows.

- The CFST frame and HSS frame with comparable seismic design exhibit similar mean values and distribution shapes of structural response under frequent and basis ground motions, with HSS frames showing slightly larger responses. Meanwhile, in rare and very rare earthquake scenarios, the collapse probability of CFST frame structure is smaller due to the enhanced ability of the filled concrete to suppress the buckling of the external steel tubes.
- Under frequent and basis ground motions, although the CFST frame may exhibit smaller structural responses, their columns have significantly lower ductility compared to HSS columns based on the formulas in the literature, potentially leading to greater post-earthquake consequences. However, under rare and very rare levels, the damage to non-structural elements becomes the primary concern, and the CFST frame structure shows advantages in this case due to smaller collapse probability.
- Due to varying costs and carbon emission factors among different components, as well as their distinct contributions to seismic consequences under different scenarios, conclusions based on economic and carbon emission indicators may not always align. Considering the life cycle seismic consequences, the CFST frame is superior to HSS frame in terms of economic indicator but is at a disadvantage in carbon emission indicator. However, when initial investment and seismic consequences are collectively considered, CFST frame demonstrates advantages in both indicators.
- The findings presented above are subject to certain simplifications and assumptions. For example, the number of floors and bays, the plan and elevation layout, etc. Uncertainties in these preset parameters can be further considered. Moreover, considering the impact of the vulnerability fragility of the CFST columns and HSS columns on the consequence analysis, a comparative study and detailed examination of the full-range capacity of these two types of components should be further investigated in the future.
- The findings are anticipated to offer stakeholders additional insights for decision-making, considering the trade-offs among various perspectives related to various structural systems. Future research can delve into the life-cycle resilience and sustainability of more structural systems or members under single or combined hazards such as earthquakes, fires, and corrosion, such as steel-reinforced concrete (SRC) structures, and partially encased concrete (PEC) structures, through more diverse means (e.g., machine learning [78,79]).

CRediT authorship contribution statement

Jiajun Du: Writing – original draft, Visualization, Validation, Software, Methodology, Investigation, Formal analysis, Data curation, Conceptualization. **Wei Wang:** Writing – review & editing, Supervision, Resources, Project administration, Funding acquisition, Conceptualization. **Shiye Wang:** Writing – original draft, Visualization, Software, Methodology, Investigation, Conceptualization.

Declaration of competing interest

The authors declare that they have no known competing financial interests or personal relationships that could have appeared to influence the work reported in this paper.

Data availability

Data will be made available on request.

Acknowledgements

The financial supports from the Natural Science Foundation of China (NSFC) with Grant Nos. 52378182 and 52078366 are gratefully acknowledged. This study is also supported by the Top Discipline Plan of Shanghai Universities-Class I with Grant No. 2022-3-YB-18 and Shanghai 2022 Science and Technology Innovation Action Plan Social Development Science and Technology Research Project with Grant No. 22dz1201700.

References

[1] AR6 Synthesis Report: Climate Change 2023 — IPCC, (n.d.). https://www.ipcc.ch/report/sixth-assessment-report-cycle/ (accessed April 19, 2024).
[2] China Association of Building Energy Efficiency, 2022 China Building Energy Consumption and Carbon Emissions Research Report, China Association of Building Energy Efficiency, Chongqing, 2022.
[3] S. Hu, Y. Koetaka, Z.-P. Chen, S. Zhu, M.S. Alam, Hybrid self-centering braces with NiTi-SMA U-shaped and frequency-dependent viscoelastic dampers for structural and nonstructural damage control, Eng. Struct. 308 (2024) 117920, https://doi.org/10.1016/j.engstruct.2024.117920.
[4] J. Du, W. Meng, K.H. Khayat, Y. Bao, P. Guo, Z. Lyu, A. Abu-obeidah, H. Nassif, H. Wang, New development of ultra-high-performance concrete (UHPC), Compos. Part B Eng. 224 (2021) 109220, https://doi.org/10.1016/j.compositesb.2021.109220.
[5] S.H.I. Gang, B.A.N. Hui-yong, S.H.I. Yong-Jiu, W. Yuan-Qing, Overview of research progress for high strength steel structures, Eng. Mech. 30 (2013) 1–13, https://doi.org/10.6052/j.issn.1000-4750.2012.05.ST10.
[6] R. Zhang, W. Wang, C. Fang, Evaluation of a full-scale friction spring-based self-centering damper considering cumulative seismic demand, J. Struct. Eng. 148 (2022) 04021281, https://doi.org/10.1061/(ASCE)ST.1943-541X.0003267.
[7] Nik D. Oikonomou, Recycled concrete aggregates, Cem. Concr. Compos. 27 (2005) 315–318, https://doi.org/10.1016/j.cemconcomp.2004.02.020.

[8] S. He, X. Zhao, E.Q. Wang, G.S. Chen, P.-Y. Chen, L. Hu, Engineered wood: sustainable technologies and applications, Annu. Rev. Mater. Res. 53 (2023) 195–223, https://doi.org/10.1146/annurev-matsci-010622-105440.

[9] Y. Chen, F. Zhou, S. Zheng, J. Li, C. Shang, X. Lin, Influence of cyclic hardening characteristic on seismic performance of welded austenitic stainless steel H-section beam-column, Eng. Struct. 288 (2023) 116210, https://doi.org/10.1016/j.engstruct.2023.116210.

[10] R. Zhang, S. Hu, Optimal design of self-centering braced frames with limited self-centering braces, J. Build. Eng. 88 (2024) 109201, https://doi.org/10.1016/j.jobe.2024.109201.

[11] L.-H. Han, Y.-F. Yang, Z. Tao, Concrete-filled thin-walled steel SHS and RHS beam-columns subjected to cyclic loading, Thin-Walled Struct. 41 (2003) 801–833, https://doi.org/10.1016/S0263-8231(03)00030-2.

[12] L.-H. Han, Y.-F. Yang, Cyclic performance of concrete-filled steel CHS columns under flexural loading, J. Constr. Steel Res. 61 (2005) 423–452, https://doi.org/10.1016/j.jcsr.2004.10.004.

[13] S. Wang, W. Wang, D.G. Lignos, Experimental Study of the Cyclic Behavior of Steel Tube in Concrete-Filled Steel Tube Members, Ce/Papers, 2023, pp. 5–10, https://doi.org/10.1002/cepa.2287.

[14] S. Wang, W. Wang, Z. Xie, Nonlinear cyclic behavior of steel tube in concrete-filled steel tube members including local buckling, Thin-Walled Struct. 191 (2023) 111055, https://doi.org/10.1016/j.tws.2023.111055.

[15] S. Gao, J. Yang, S. Kang, F. Li, X. Shi, Experimental and numerical studies on deformation performance of square concrete-filled steel tubular columns under repeated lateral impacts, Eng. Struct. 308 (2024) 117909, https://doi.org/10.1016/j.engstruct.2024.117909.

[16] Q.-Y. Song, L.-H. Han, K. Zhou, Y. Feng, Fire resistance of circular concrete-filled steel tubular (CFST) column protected by intumescent coating, J. Constr. Steel Res. 147 (2018) 154–170, https://doi.org/10.1016/j.jcsr.2018.03.038.

[17] K. Zhou, L.-H. Han, Modelling the behaviour of concrete-encased concrete-filled steel tube (CFST) columns subjected to full-range fire, Eng. Struct. 183 (2019) 265–280, https://doi.org/10.1016/j.engstruct.2018.12.100.

[18] S. Li, L.-H. Han, F.-C. Wang, C.-C. Hou, Seismic behavior of fire-exposed concrete-filled steel tubular (CFST) columns, Eng. Struct. 224 (2020) 111085, https://doi.org/10.1016/j.engstruct.2020.111085.

[19] L.-H. Han, C.-C. Hou, Q.-L. Wang, Behavior of circular CFST stub columns under sustained load and chloride corrosion, J. Constr. Steel Res. 103 (2014) 23–36, https://doi.org/10.1016/j.jcsr.2014.07.021.

[20] C.-C. Hou, L.-H. Han, Q.-L. Wang, C. Hou, Flexural behavior of circular concrete filled steel tubes (CFST) under sustained load and chloride corrosion, Thin-Walled Struct. 107 (2016) 182–196, https://doi.org/10.1016/j.tws.2016.02.020.

[21] M. Hastak, D.W. Halpin, Assessment of life-cycle benefit-cost of composites in construction, J. Compos. Constr. 4 (2000) 103–111, https://doi.org/10.1061/(ASCE)1090-0268(2000)4:3(103).

[22] B. Rossi, I. Lukić, N. Iqbal, G. Du, D. Cregg, R. Borg, P. Haller, Life cycle impacts assessment of steel, composite, concrete and wooden columns, in: Final Int. Conf. COST Action C25 - Sustain. Constr, Better Built Environ, Innsbruck, Austria, 2011, pp. 277–285.

[23] M. Zhao, Y. Dong, Comparative life cycle assessment of composite structures incorporating uncertainty and global sensitivity analysis, Eng. Struct. 242 (2021) 112394, https://doi.org/10.1016/j.engstruct.2021.112394.

[24] R.E. Gonzalez, M.T. Stephens, C. Toma, D. Dowdell, The estimated carbon cost of concrete building demolitions following the Canterbury earthquake sequence, Earthquake Spectra 38 (2022) 1615–1635, https://doi.org/10.1177/87552930221082684.

[25] C. Pan, H. Wang, S. Huang, H. Zhang, The great East Japan earthquake and tsunami aftermath: Preliminary assessment of carbon footprint of housing reconstruction, in: Y.A. Kontar, V. Santiago-Fandiño, T. Takahashi (Eds.), Tsunami Events Lessons Learn. Environ. Soc. Significance, Springer, Netherlands, Dordrecht, 2014, pp. 435–450, https://doi.org/10.1007/978-94-007-7269-4_25.

[26] R.E. Gonzalez, M.T. Stephens, C. Toma, D. Dowdell, Incorporating potential environmental impacts in building seismic design decisions, Bull. Earthq. Eng. 21 (2023) 4385–4428, https://doi.org/10.1007/s10518-023-01686-y.

[27] J. Du, W. Wang, T. Lou, H. Zhou, Resilience and sustainability-informed probabilistic multi-criteria decision-making framework for design solutions selection, J. Build. Eng. 71 (2023) 106421, https://doi.org/10.1016/j.jobe.2023.106421.

[28] G.A. Anwar, Y. Dong, Y. Li, Performance-based decision-making of buildings under seismic hazard considering long-term loss, sustainability, and resilience, Struct. Infrastruct. Eng. 17 (2021) 454–470, https://doi.org/10.1080/15732479.2020.1845751.

[29] K.M. Mosalam, U. Alibrandi, H. Lee, J. Armengou, Performance-based engineering and multi-criteria decision analysis for sustainable and resilient building design, Struct. Saf. 74 (2018) 1–13, https://doi.org/10.1016/j.strusafe.2018.03.005.

[30] K. Angeles, D. Patsialis, A.A. Taflanidis, T.L. Kijewski-Correa, A. Buccellato, C. Vardeman, Advancing the Design of Resilient and Sustainable Buildings: an integrated life-cycle analysis, J. Struct. Eng. 147 (2021) 04020341, https://doi.org/10.1061/(ASCE)ST.1943-541X.0002910.

[31] S. Hu, S. Zhu, Life-cycle benefits estimation for hybrid seismic-resistant self-centering braced frames, Earthq. Eng. Struct. Dyn. 52 (2023) 3097–3119, https://doi.org/10.1002/eqe.3914.

[32] S. Hu, W. Wang, M. Shahria Alam, K. Ke, Life-cycle benefits estimation of self-centering building structures, Eng. Struct. 284 (2023) 115982, https://doi.org/10.1016/j.engstruct.2023.115982.

[33] S. Hu, R. Zhang, M.S. Alam, Z. Ding, Post-earthquake repairability enhancement of BRBFs considering isotropic hardening with self-centering braces, J. Constr. Steel Res. 217 (2024) 108638, https://doi.org/10.1016/j.jcsr.2024.108638.

[34] R. Zhang, W. Wang, M.S. Alam, Seismic evaluation of friction spring-based self-centering braced frames based on life-cycle cost, Earthq. Eng. Struct. Dyn. (2022), https://doi.org/10.1002/eqe.3728.

[35] A.Y. Al-Attraqchi, M.J. Hashemi, R. Al-Mahaidi, Loss assessment of rigid-frame bridges under horizontal and vertical ground motions, Structures 35 (2022) 243–259, https://doi.org/10.1016/j.istruc.2021.11.014.

[36] H.S. Park, J.W. Hwang, B.K. Oh, Integrated analysis model for assessing CO2 emissions, seismic performance, and costs of buildings through performance-based optimal seismic design with sustainability, Energ. Build. 158 (2018) 761–775, https://doi.org/10.1016/j.enbuild.2017.10.070.

[37] M. Caruso, R. Pinho, F. Bianchi, F. Cavalieri, M.T. Lemmo, A life cycle framework for the identification of optimal building renovation strategies considering economic and environmental impacts, Sustainability 12 (2020) 10221, https://doi.org/10.3390/su122310221.

[38] N. Clemett, W.W. Carofilis Gallo, G. Gabbianelli, G.J. O'Reilly, R. Monteiro, Optimal combined seismic and energy efficiency retrofitting for existing buildings in Italy, J. Struct. Eng. 149 (2023), https://doi.org/10.1061/(ASCE)ST.1943-541X.0003500.

[39] C. Menna, L. Felicioni, P. Negro, A. Lupíšek, E. Romano, A. Prota, P. Hájek, Review of methods for the combined assessment of seismic resilience and energy efficiency towards sustainable retrofitting of existing European buildings, Sustain. Cities Soc. 77 (2022) 103556, https://doi.org/10.1016/j.scs.2021.103556.

[40] H. Krawinkler, E. Miranda, Performance-based earthquake engineering, Earthq. Eng. Eng. Seismol. Perform.-Based Eng. 9 (2004) 1–9.

[41] FEMA, Hazus Earthquake Model Technical Manual - Hazus 5.1. https://www.fema.gov/sites/default/files/documents/fema_hazus-earthquake-model-technical-manual-5-1.pdf, 2022 (accessed May 9, 2023).

[42] FEMA, FEMA P-58:Seismic Performance Assessment of Buildings, Second edition, FEMA, Washington, DC, 2018.

[43] I. Almufti, M. Willford, REDi™ Rating System: Resilience-based Earthquake Design Initiative for the Next Generation of Buildings, Arup Co, 2013.

[44] Standardization Administration of the P.R.C, GB/T38591-2020 Standard for Seismic Resilience Assessment of Buildings, 2020.

[45] Standardization Administration of the P.R.C, GB18306-2015: Seismic Ground Motion Parameters Zonation Map of China, 2015.

[46] C. Liu, D. Lu, Probabilistic seismic Hazard analysis for China based on Bayesian network, Seismol. Res. Lett. 95 (2023) 50–63, https://doi.org/10.1785/0220230159.

[47] T. Lin, C.B. Haselton, J.W. Baker, Conditional spectrum-based ground motion selection. Part I: Hazard consistency for risk-based assessments, Earthq. Eng. Struct. Dyn. 42 (2013) 1847–1865, https://doi.org/10.1002/eqe.2301.

[48] T. Lin, C.B. Haselton, J.W. Baker, Conditional spectrum-based ground motion selection. Part II: intensity-based assessments and evaluation of alternative target spectra, Earthq. Eng. Struct. Dyn. 42 (2013) 1867–1884, https://doi.org/10.1002/eqe.2303.

[49] V. Hasik, J.P.S. Chhabra, G.P. Warn, M.M. Bilec, Review of approaches for integrating loss estimation and life cycle assessment to assess impacts of seismic building damage and repair, Eng. Struct. 175 (2018) 123–137, https://doi.org/10.1016/j.engstruct.2018.08.011.

[50] Ministry of Housing and Urban-Rural Development of the People''s Republic of China, GB/T51366-2019: Standard for Building Carbon Emission Calculation, 2019.

[51] China Building Decoration Association, Standard for Building Decoration Carbon Emission Calculation, 2022.

[52] Jiangsu Provincial Department of Housing and Urban-Rural Development, Building Carbon Emission Calculation Guidelines of Jiangsu Province, (n.d.).

[53] K. Simonen, S. Merrifield, I. Almufti, K. Strobel, J. Tipler, Integrating Environmental Impacts as Another Measure of Earthquake Performance for Tall Buildings in High Seismic Zones, 2015, pp. 933–944, https://doi.org/10.1061/9780784479117.080.

[54] M.V. Comber, C. Poland, M. Sinclair, Environmental Impact Seismic Assessment: Application of Performance-Based Earthquake Engineering Methodologies to Optimize Environmental Performance, 2012, pp. 910–921, https://doi.org/10.1061/9780784412367.081.

[55] J.E. Padgett, Y. Li, Risk-based assessment of sustainability and Hazard resistance of structural design, J. Perform. Constr. Facil. 30 (2016) 04014208, https://doi.org/10.1061/(ASCE)CF.1943-5509.0000723.

[56] C.K. Chiu, M.R. Chen, C.H. Chiu, Financial and environmental payback periods of seismic retrofit investments for reinforced concrete buildings estimated using a novel method, J. Archit. Eng. 19 (2013) 112–118, https://doi.org/10.1061/(ASCE)AE.1943-5568.0000105.

[57] C. Feese, Y. Li, W.M. Bulleit, Assessment of seismic damage of buildings and related environmental impacts, J. Perform. Constr. Facil. 29 (2015) 04014106, https://doi.org/10.1061/(ASCE)CF.1943-5509.0000584.

[58] H.-H. Wei, M.J. Skibniewski, I.M. Shohet, X. Yao, Lifecycle environmental performance of natural-Hazard mitigation for buildings, J. Perform. Constr. Facil. 30 (2016) 04015042, https://doi.org/10.1061/(ASCE)CF.1943-5509.0000803.

[59] C. Menna, D. Asprone, F. Jalayer, A. Prota, G. Manfredi, Assessment of ecological sustainability of a building subjected to potential seismic events during its lifetime, Int. J. Life Cycle Assess. 18 (2013) 504–515, https://doi.org/10.1007/s11367-012-0477-9.

[60] B. Gencturk, K. Hossain, S. Lahourpour, Life cycle sustainability assessment of RC buildings in seismic regions, Eng. Struct. 110 (2016) 347–362, https://doi.org/10.1016/j.engstruct.2015.11.037.
[61] A. Belleri, A. Marini, Does seismic risk affect the environmental impact of existing buildings? Energ. Build. 110 (2016) 149–158, https://doi.org/10.1016/j.enbuild.2015.10.048.
[62] YJK software, (n.d.). https://www.yjk.cn/ (accessed April 23, 2024).
[63] Z. Xu, Study on Selection of Ground Motion Records in Code for Seismic Design of Buildings, Doctoral Dissertation, Institute of Engineering Mechanics, China Earthquake Administration, 2021.
[64] F. McKenna, OpenSees: a framework for earthquake engineering simulation, Comput. Sci. Eng. 13 (2011) 58–66, https://doi.org/10.1109/MCSE.2011.66.
[65] L.F. Ibarra, R.A. Medina, H. Krawinkler, Hysteretic models that incorporate strength and stiffness deterioration, Earthq. Eng. Struct. Dyn. 34 (2005) 1489–1511, https://doi.org/10.1002/eqe.495.
[66] D.G. Lignos, H. Krawinkler, Deterioration modeling of steel components in support of collapse prediction of steel moment frames under earthquake loading, J. Struct. Eng.-Rest. 137 (2011) 1291.
[67] H. El Jisr, A. Elkady, D.G. Lignos, Hysteretic behavior of moment-resisting frames considering slab restraint and framing action, J. Struct. Eng. 146 (2020) 04020145, https://doi.org/10.1061/(ASCE)ST.1943-541X.0002696.
[68] L. Han, Concrete Filled Steel Tubular Structures-Theory and Practice, Third edition, Science Press, Beijing, 2016.
[69] Concrete01 Material – Zero Tensile Strength - OpenSeesWiki, (n.d.). https://opensees.berkeley.edu/wiki/index.php/Concrete01_Material_–_Zero_Tensile_Strength (accessed April 24, 2024).
[70] C. Tort, J.F. Hajjar, Mixed finite-element modeling of rectangular concrete-filled steel tube members and frames under static and dynamic loads, J. Struct. Eng. 136 (2010) 654–664, https://doi.org/10.1061/(ASCE)ST.1943-541X.0000158.
[71] S. Wang, W. Wang, D.G. Lignos, Uniaxial material model with softening for simulating the cyclic behavior of steel tubes in concrete filled steel tube beam-columns, Earthq. Eng. Struct. Dyn. n.d. (Under Review).
[72] J.L. Chaboche, A review of some plasticity and viscoplasticity constitutive theories, Int. J. Plast. 24 (2008) 1642–1693, https://doi.org/10.1016/j.ijplas.2008.03.009.
[73] M. Rahnama, H. Krawinkler, Effects of Soft Soil and Hysteresis Model on Seismic Demands. https://purl.stanford.edu/xr254mk7856, 1993 (accessed April 28, 2024).
[74] E. Inai, A. Mukai, M. Kai, H. Tokinoya, T. Fukumoto, K. Mori, Behavior of concrete-filled steel tube beam columns, J. Struct. Eng. 130 (2004) 189–202, https://doi.org/10.1061/(ASCE)0733-9445(2004)130:2(189).
[75] Y. Suzuki, D.G. Lignos, Experimental evaluation of steel columns under seismic Hazard-consistent collapse loading protocols, J. Struct. Eng. 147 (2021) 04021020, https://doi.org/10.1061/(ASCE)ST.1943-541X.0002963.
[76] Program for Seismic Resilience Assessment of Buildings, (n.d.). http://www.kangzhenhulian.com/ (accessed April 25, 2024).
[77] CPCD, China Products Carbon Footprint Factors Database, (n.d.). https://lca.cityghg.com/pages/index (accessed April 25, 2024).
[78] S. Hu, W. Wang, Y. Lu, Explainable machine learning models for probabilistic buckling stress prediction of steel shear panel dampers, Eng. Struct. 288 (2023) 116235, https://doi.org/10.1016/j.engstruct.2023.116235.
[79] S. Hu, W. Wang, M.S. Alam, S. Zhu, K. Ke, Machine learning-aided peak displacement and floor acceleration-based design of hybrid self-centering braced frames, J. Build. Eng. 72 (2023) 106429, https://doi.org/10.1016/j.jobe.2023.106429.